FULL PAPER

Theranostic USPIO-Loaded Microbubbles for Mediating and Monitoring Blood-Brain Barrier Permeation

Twan Lammers, Patrick Koczera,* Stanley Fokong, Felix Gremse, Josef Ehling, Michael Vogt, Andrij Pich, Gert Storm, Marc van Zandvoort, and Fabian Kiessling**

Efficient and safe drug delivery across the blood-brain barrier (BBB) remains one of the major challenges of biomedical and (nano-) pharmaceutical research. Here, it is demonstrated that poly(butyl cyanoacrylate)-based microbubbles (MB), carrying ultrasmall superparamagnetic iron oxide (USPIO) nanoparticles within their shell, can be used to mediate and monitor BBB permeation. Upon exposure to transcranial ultrasound pulses, USPIO-MB are destroyed, resulting in acoustic forces inducing vessel permeability. At the same time, USPIO are released from the MB shell, they extravasate across the permeabilized BBB and they accumulate in extravascular brain tissue, thereby providing non-invasive R_2*-based magnetic resonance imaging information on the extent of BBB opening. Quantitative changes in R_2* relaxometry are in good agreement with 2D and 3D microscopy results on the extravascular deposition of the macromolecular model drug fluorescein isothiocyanate (FITC)-dextran into the brain. Such theranostic materials and methods are considered to be useful for mediating and monitoring drug delivery across the BBB and for enabling safe and efficient treatment of CNS disorders.

1. Introduction

The blood-brain barrier (BBB) is the primary obstacle for treating diseases of the central nervous system (CNS).[1,2] It consists of closely packed endothelial cells, pericytes, astrocytes, tight junctions, and extracellular matrix components, which together line cerebral blood vessels and prevent the vast majority of therapeutic and toxic compounds from entering the CNS.[3,4] Several different strategies have been evaluated for enhancing drug delivery across the BBB, including e.g., pharmacological modulation, via the intra-arterial injection of hyperosmotic fluids such as mannitol,[5] or pharmaceutical optimization, via the design of drug delivery systems targeted to receptors (over-) expressed by brain endothelial cells, such as the transferrin receptor, to enable active carrier-mediated transport across the BBB.[2,5–8]

In recent years, also ultrasound (US)-based techniques have started to attract significant attention for enhancing drug delivery across the BBB.[9–13] The use of US to permeabilize vascular endothelium and cellular membranes is referred to as sonoporation, and it is known to profit substantially from the concomitant use of microbubbles (MB). MB are 1 to 5 µm-sized gas- or air-filled vesicles stabilized by lipids, polymers or proteins, and they are routinely used as US contrast agents. MB substantially reduce the acoustic forces needed to induce sonoporation. In addition to permeabilizing vascular and cellular membranes, MB have also been employed for thrombolysis and for "direct" drug

Prof. T. Lammers, P. Koczera, Dr. S. Fokong,
F. Gremse, Dr. J. Ehling, Prof. F. Kiessling
Department for Experimental Molecular Imaging
University Clinic and Helmholtz Institute for Biomedical Engineering
RWTH Aachen University
Pauwelsstrasse 20, 52074, Aachen, Germany
E-mail: tlammers@ukaachen.de; pkoczera@ukaachen.de;
fkiessling@ukaachen.de
Prof. T. Lammers, Prof. G. Storm
Department of Controlled Drug Delivery
MIRA Institute for Biomedical Engineering and Technical Medicine
University of Twente
Enschede, The Netherlands
Prof. T. Lammers, Prof. G. Storm
Department of Pharmaceutics
Utrecht Institute for Pharmaceutical Sciences
Utrecht University
Utrecht, The Netherlands
Dr. M. Vogt, Prof. M. van Zandvoort
Institute for Molecular Cardiovascular
Research (IMCAR)
University Clinic
RWTH Aachen University
Aachen, Germany
Prof. A. Pich
Functional and Interactive Polymers
DWI, Leibniz Centre for Interactive Materials
RWTH Aachen University
Aachen, Germany
Prof. M. van Zandvoort
Department of Genetics and Cell Biology
Cardiovascular Research Institute Maastricht (CARIM)
Maastricht University
Maastricht, The Netherlands

DOI: 10.1002/adfm.201401199

delivery, upon loading low-molecular-weight or nucleic acid-based therapeutics into or onto their shell, and then locally triggering the release, extravasation and/or internalization of the incorporated or attached therapeutic agents upon exposure to destructive US pulses.[14–20]

Remarkably, the majority of efforts in this area of research have focused on enhancing drug delivery to tumors and tumor cells, in spite of the fact that angiogenic blood vessels in tumors are known to already be relatively leaky. Conversely, when considering that the most debilitating CNS disorders, such as Alzheimer and Parkinson's disease, can potentially only be curatively treated with macromolecular drugs, such as growth factors, there appears to be an obvious need for establishing materials and methods to permeate the BBB and to do so in a quantifiable and controllable manner, ideally via non-invasive imaging guidance.

Here, we employed poly(*n*-butyl-cyanoacrylate) (PBCA)-based MB, containing ultrasmall super-paramagnetic iron oxide (USPIO) nanoparticles within their polymeric shell, to at the same time mediate and monitor BBB permeation. Shell-incorporated USPIO and fluorophores are known to be efficiently released upon US-mediated MB destruction.[18,21] Based on this, we reasoned that magnetic resonance imaging (MRI) of USPIO release from MB and their subsequent extravascular deposition into the CNS might be a suitable means for non-invasively assessing BBB permeation.

As exemplified by **Figure 1**, USPIO-containing MB were i.v. infused into healthy mice and transcranially destroyed using high mechanical index US pulses. The accumulation of released and extravasated USPIO in brain tissue was visualized and quantified using MRI. In parallel, the delivery of the 70 kDa macromolecular model drug fluorescein isothiocyanate (FITC)-dextran across the BBB was monitored using 2D and 3D microscopy techniques, confirming that US-mediated MB destruction enables efficient drug delivery relatively deep into the brain. Such theranostic strategies, in which diagnostic materials and methods are used to deliver therapeutic entities across the BBB in a controllable and quantifiable manner, are considered to be highly useful for efficiently and (more) safely delivering drugs to the CNS, providing real-time feedback on the degree of BBB opening, and thereby minimizing the chances of doing damage to healthy brain tissue (as a result of over-permeation, e.g., bleedings, inflammation and edema formation).

2. Results and Discussion

USPIO nanoparticles were incorporated into the shell of PBCA-based MB using a one-pot synthetic procedure (**Figure 2**A). Coulter counter measurements showed that the average diameter of the MB was ≈2.5 µm, and scanning electron microscopy (SEM) indicated a shell thickness of ≈50 nm (Figure 2B–D). The shell thickness of the USPIO-MB was found to be comparable to that of regular MB (56 ± 5 vs. 48 ± 8 nm, respectively; Supporting Information Table S1). The transmission electron microscopy (TEM) images in Figure 2E–H confirm the efficient embedding of USPIO into the MB shell. Using inductively coupled mass spectrometry (ICP-MS), it was demonstrated that each individual MB contained ≈15 fg of iron, corresponding to an encapsulation efficiency of ≈40%.[21] The amount of iron per MB remained stable for >6 months, confirming a proper shelf-life. The colloidal stability of the USPIO-MB was assessed using zeta potential and creaming velocity analyses, showing that upon USPIO embedding, both the zeta potential (–42 ± 4.4 vs. –38 ± 5.9 mV) and the creaming velocity (6 ± 0.9 vs. 11 ±

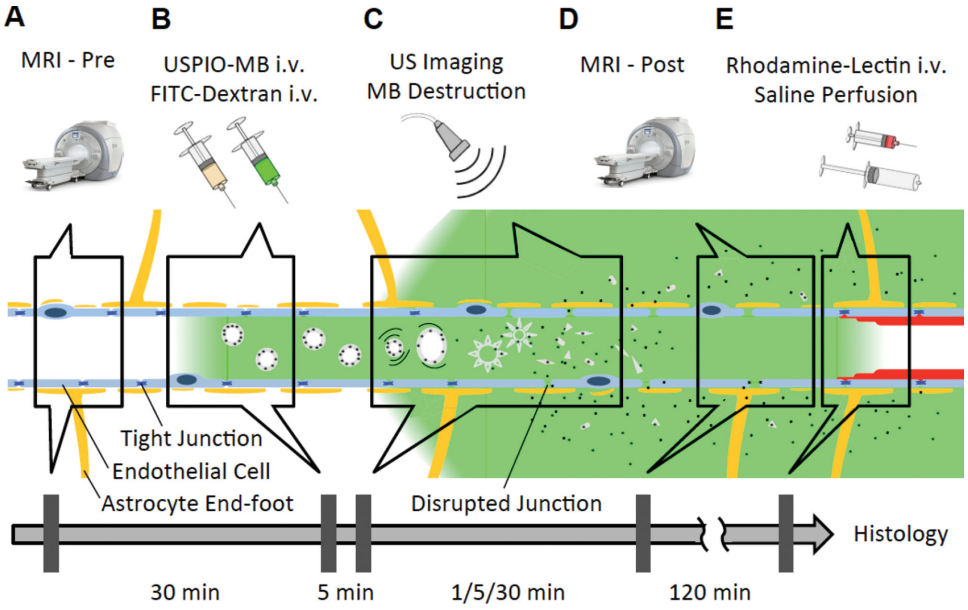

Figure 1. Schematic experimental setup for mediating and monitoring drug delivery across the BBB using USPIO-loaded MB. After an MRI pre-scan (A), USPIO-MB and 70 kDa FITC-dextran were co-injected (B). Then, the USPIO-MB were destroyed using US, resulting in the generation of acoustic forces, USPIO release from the MB, permeation of the BBB, and USPIO extravasation (C). After an MRI post scan, to visualize and quantify USPIO deposition in the brain (D), rhodamine-lectin was injected and FITC-dextran extravasation and penetration was assessed using 2D and 3D microscopy (E).

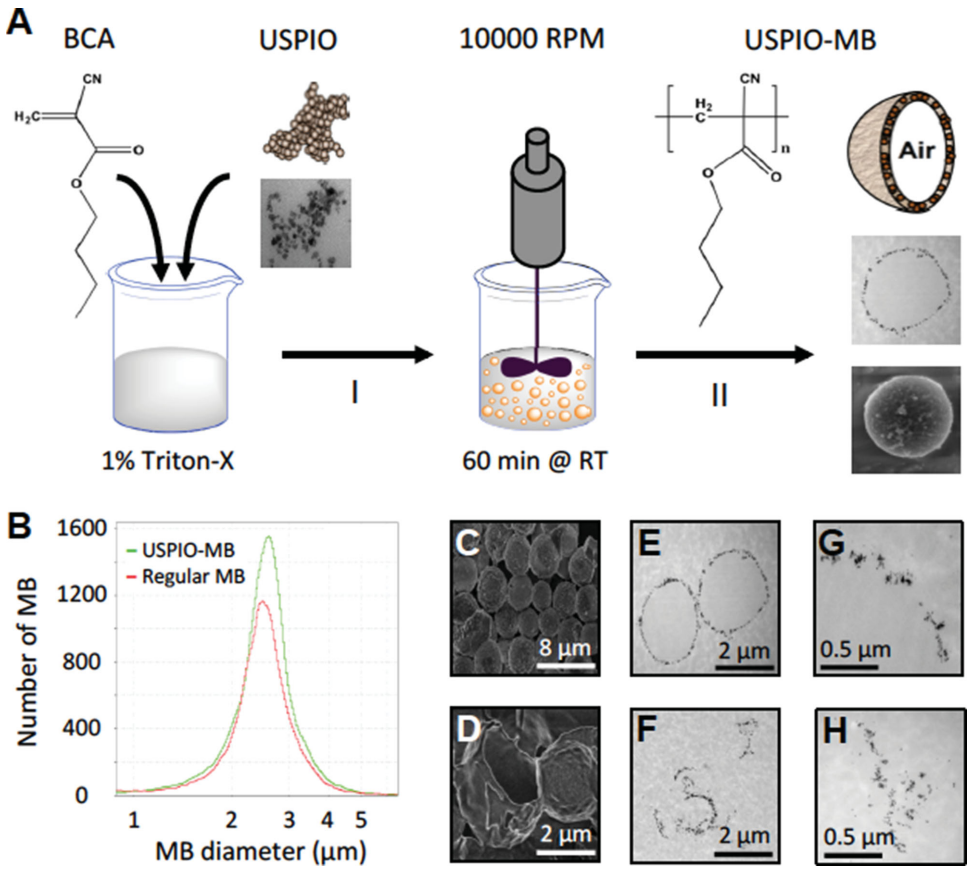

Figure 2. Synthesis and characterization of USPIO-loaded MB. A) Schematic synthetic protocol. B) Size and size distribution of USPIO-loaded and regular MB. C–H) SEM and TEM images of intact (C,E,G) and destroyed (D,F,H) USPIO-MB, exemplifying an average diameter of ≈2.5 μm, a shell thickness of ≈50 nm, efficient USPIO incorporation into the shell, and (partial) USPIO release upon US-mediated MB destruction. See Supporting Information Table S1 for more details.

1.0 μm s^{-1}) slightly decreased, which indicates that USPIO incorporation slightly increases the stability of the dispersion (Supporting Information Table S1). Furthermore, in phantom experiments, a significant decrease in relaxation times was observed upon the US-mediated destruction of USPIO-MB, which results from the (partial) release of USPIO nanoparticles from the MB shell.[21] This notion is in line with the TEM images in Figure 2E–H, which also clearly indicate that upon exposure to destructive US pulses, partof the entrapped iron is released from the MB shell.

Upon i.v. infusion, USPIO-containing MB could be readily detected in the brain of mice, using power Doppler US imaging (**Figure 3**A, Supporting Information Video S1). To visualize and quantify BBB permeation, morphological T_2*-weighted MR images and T_2*-relaxometry of the brain of mice (n = 5 per group) were acquired before and after USPIO-MB administration and exposure to destructive US pulses (for 1, 5 and 30 min). Control mice received either USPIO-MB alone or US alone. As shown in Figure 3B,C, a significant increase in R_2* relaxation rates was observed for animals treated with both USPIO-MB and US. One minute of US in combination with USPIO-MB resulted in an insignificant increase in R_2* values (by 5.5%; $p = 0.11$), while 5 and 30 min of US plus USPIO-MB highly significantly ($p < 0.01$) increased the R_2* values vs. baseline, by 14.4% and 21.0%, respectively. No significant differences vs. baseline were observed in control groups. In line with this, for the latter two, analysis of variance (ANOVA) testing vs. the respective control groups showed highly significant increases in R_2* ($p < 0.0001$). USPIO-MB plus 5 min of US resulted in higher R_2* values than 5 min of US alone and USPIO-MB alone, and USPIO-MB plus 30 min of US presented with higher values than 30 min of US alone and USPIO-MB alone (Figure 3C). USPIO deposition across the BBB and into the CNS was confirmed using post-mortem Prussian blue staining (Figure 3D). These findings indicate that the USPIO nanoparticles embedded in the MB shell can be used to quantitatively assess the degree of BBB permeation, using a 3T clinical MR scanner.

To rule out the possibility of treatment-induced brain edema formation, the T_2-based FLAIR (fluid-attenuated inversion recovery) sequence was used, which enables edema assessment. As shown in Supporting Information Figure S1, no hint towards the induction of brain edema in any of the treatment groups was found. Since the blood half-life time of MB is known to be in the order of 1–2 min,[22] and since the post-US MR scans were obtained at 40 min after USPIO-MB injection, the observed increases in R_2* values can therefore be considered to truly reflect USPIO extravasation across the BBB, rather

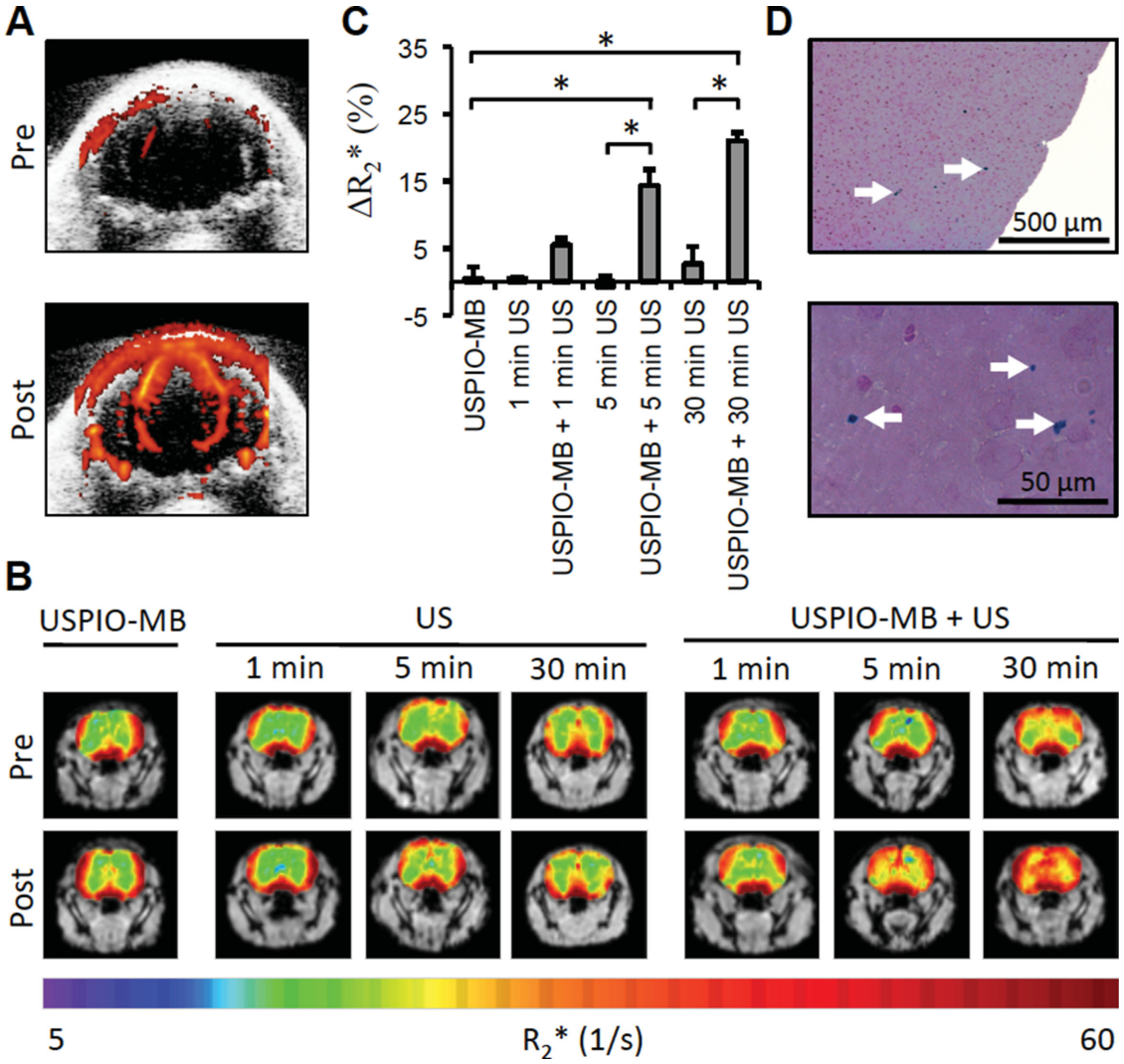

Figure 3. Mediating and monitoring BBB permeation using USPIO-MB. A) Power Doppler US images before and directly after the i.v. infusion of USPIO-MB. B) MR imaging of USPIO deposition across the BBB upon US-induced USPIO-MB destruction. Color-coded R_2*-maps are overlaid on morphological T_2*-weighted images, which were recorded before and after exposure to US. C) Quantification of the increase in R_2* values, presented as percentage ± SEM. * indicates $p < 0.0001$ vs. USPIO-MB alone and US alone. D) Prussian Blue staining of brain tissue, confirming the deposition of USPIO nanoparticles (arrows) across the BBB and within the CNS.

than USPIO-MB still circulating in cerebral blood vessels. Microhemorrhages as a cause for changes in R_2* can also be excluded, as sonication with USPIO-free MB did not alter R_2* values (Supporting Information Figure S2A,B).

To demonstrate that the developed hybrid materials are more efficient for mediating and monitoring BBB permeation than is the separate application of USPIO nanoparticles and MB, we co-administered a comparable amount of regular MB with a clinically relevant concentration of Resovist (i.e., carboxydextran-coated SPIO), and exposed the animals to 5 min of US. As additional controls, Resovist was also administered alone, as well as in combination with only MB and only US. As shown in Supporting Information Figure S2C,D, neither of these conditions resulted in a significant increase in R_2* values, in spite of the fact that a >5 higher amount of iron was injected in case of Resovist as compared to USPIO-MB (70 vs. 13 µg, respectively).

To evaluate if the USPIO-MB- plus US-induced opening of the BBB enables macromolecular drug delivery to the brain, the fluorescent model drug FITC-dextran (70 kDa) was i.v. injected directly before USPIO-MB infusion, and prior to exposure to transcranial US. To facilitate the 2D fluorescence microscopy (2D-FM) and 3D two-photon laser scanning microscopy (3D-2PM) analyses of FITC-dextran extravasation, rhodamine-lectin was i.v. injected, to enable intravital staining of functional blood vessels in the brain. Prior to sacrificing the animals and harvesting brain tissue, they received an i.p. injection of heparin (to prevent blot clotting) and they were intracardially perfused with PBS (to remove intravascular FITC-dextran). As shown in the upper panels in **Figure 4**A, in line with the MRI analyses, in animals treated with USPIO-MB plus 5 and 30 min of US, very bright signals corresponding to extravasated FITC-dextran could be observed using 2D-FM, always surrounding perfused and rhodamine-labeled blood vessels. In control animals, as

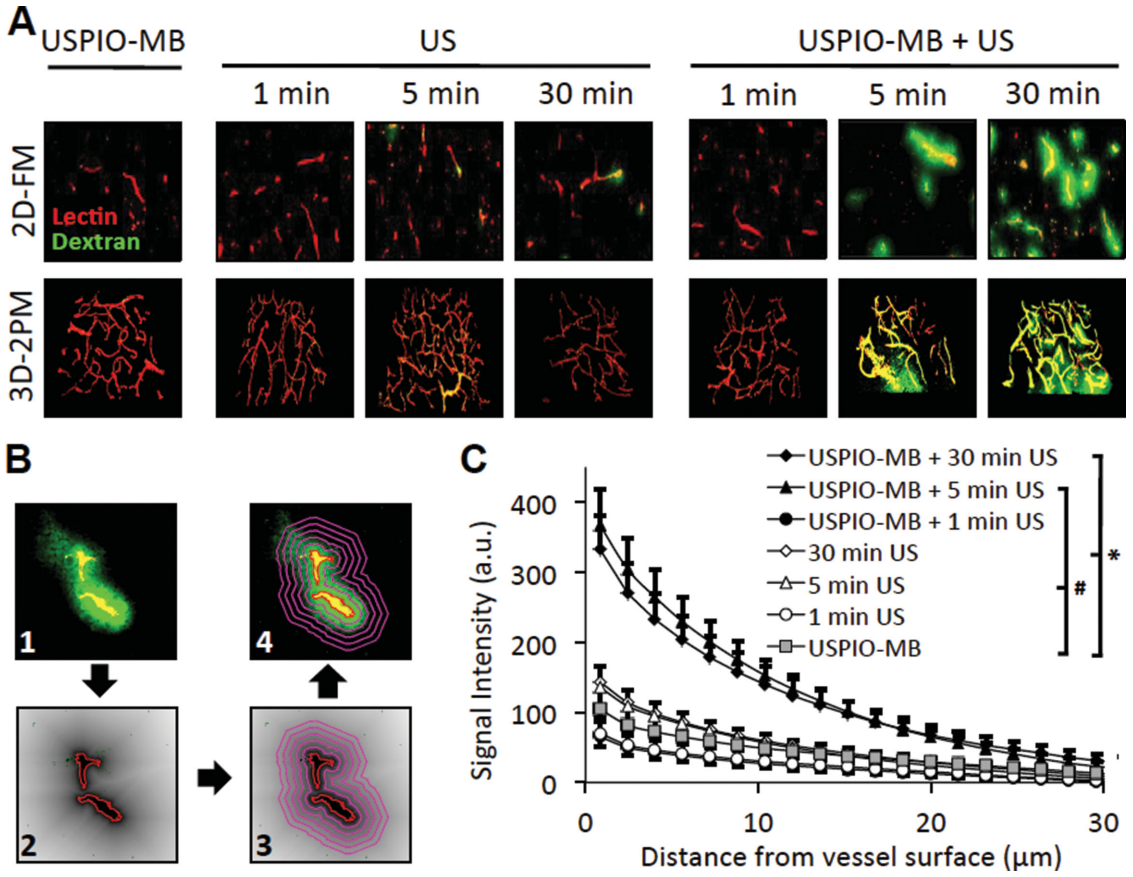

Figure 4. FITC-dextran extravasation and penetration. A) 2D fluorescence (2D-FM) and 3D two-photon microscopy (3D-2PM) of FITC-dextran (green) extravasation across rhodamin-lectin-stained (red) blood vessels, showing efficient macromolecular (model) drug delivery across the BBB upon the combination of USPIO-MB with 5 and 30 min of US. B) Extravasation and penetration were quantified using a procedure in which 1) vessels were segmented by rhodamine-lectin-thresholding, 2) a distance map was calculated, 3) concentric rings were drawn around the vessels, and 4) the signal intensity of FITC-dextran was measured within each ring. C) Signal intensity of extravasated FITC-dextran as a function of distance to vessel surface. Values represent the mean signal intensity within each concentric rings ± SEM. * and # indicate $p < 0.005$ vs. USPIO-MB alone and US alone.

well as in animals treated with USPIO-MB plus 1 min of US, no significant FITC-dextran extravasation could be detected. These findings were validated using 3D-2PM (lower panels in Figure 4A), clearly confirming that USPIO-MB in combination with 5 and 30 min of US induced highly efficient FITC-dextran delivery across the BBB.

To quantitatively assess the extent of FITC-dextran extravasation across the BBB and its penetration into the CNS, an automated image analysis method was developed in which an algorithm first identifies and segments blood vessels on the basis of the rhodamine-lectin signal, and subsequently calculates distance maps (20 concentric rings; 10 pixels in depth) around each blood vessel (Figure 4B). Within each of these rings, the average signal intensity of FITC-dextran was quantified, and compared for 30 images from three brain sections for all $n = 5$ animals in each of the 7 treatment groups. The results of these analyses, in which the signal intensity of FITC-dextran is described as a function of distance from the vessel surface, are depicted in Figure 4C. As can be clearly seen, in line with the findings obtained using quantitative MRI (Figure 3B,C) and qualitative 2D and 3D microscopy (Figure 4A), in animals treated with USPIO-MB plus 5 and 30 min of US, the signal intensity of extravasated FITC-dextran was significantly higher ($p < 0.005$) than that in all other treatment groups (Figure 3C). Thus, it can be concluded that the local destruction of USPIO-MB via transcranial US enhances the permeability of the BBB, and that the extent of BBB opening is large enough to enable efficient extravasation and penetration of 5–10 nm-sized (70 kDa) macromolecular model drugs into the CNS.

Using USPIO-containing MB in combination with transcranial US, we here provide proof-of-principle for a theranostic nano-in-micromaterial that enables the simultaneous induction and imaging of BBB permeation (Figures 1 and 2). Such advanced nano- and microtheranostic materials are considered to be highly useful for improving both disease diagnosis and disease treatment.[23–26] The non-invasive imaging insights obtained here using MRI and post-mortem Prussian Blue staining showed significant USPIO deposition in the brain upon combining USPIO-MB with 5 and 30 min of US (Figure 3), and 2D and 3D microscopy techniques confirmed that USPIO-MB-mediated BBB permeation significantly improves the delivery of the 5–10 nm-sized macromolecular model drug FITC-dextran into the CNS (Figure 4). Conversely, when combining USPIO-MB with 1 min of US, no significant increases

in BBB opening could be observed, using either MRI or 2D and 3D microscopy (Figure 3, 4). This illustrates that in this particular experimental setup, the minimal US duration for efficient MB-mediated BBB permeation is somewhere between 1 and 5 min. It also shows that non-invasive MR imaging, on a clinical 3T scanner, can be used to report on (and eventually potentially tailor) BBB permeation using USPIO-MB. In this regard, it should be kept in mind that the USPIO-MB used in this study are prepared using prototypic, safe, well-characterized and clinically relevant materials. USPIO- and PBCA-based nano- and micromaterials have been extensively evaluated over the years, both in animal models and in patients,[27,28] and the required soft- and hardware tools required for performing simultaneous MR-guided HIFU (high-intensity focused ultrasound) are becoming increasingly more accessible.

Surely, for enabling safe and efficient image-guided drug delivery across the BBB, several parameters can still be further refined, including, e.g., MB-related properties (such as MB size, shell-thickness, USPIO-loading, circulation time, surface-coating and active targeting), US-related properties (such as power, duration, frequency and high-intensity focusing),[29] and MRI-related properties (such as higher-field MR scanners and optimized methods to sensitively detect subtle changes in T_2*, ideally in real-time, in a device enabling simultaneous US treatment and MR imaging). Thus, with still plenty of room for future optimization, our results indicate that relatively simple and straightforward theranostic materials and methods can be used to mediate and monitor BBB permeation, thereby substantially facilitating temporally and spatially targeted drug delivery (in-) to the CNS.

Our findings agree with several previous efforts focusing on the use of MB plus US for enabling image-guided and improved drug delivery across the BBB. Kinoshita, Hynynen, and colleagues, for instance, showed that the CNS accumulation of macromolecular anticancer agents, such as Herceptin, can be predicted on the basis of non-invasive MR imaging of the BBB penetration of a co-administered low-molecular-weight gadolinium-based contrast agent,[10] and Marty and co-workers demonstrated that differently sized MR contrast agents can be employed to non-invasively assess the duration and extent of BBB opening.[30] The advantage of using theranostic USPIO-loaded MB for mediating and monitoring BBB permeation lies in the fact that only a single agent needs to be administered to mediate and monitor BBB permeation, that the overall dose of the MR contrast agent injected can be minimized, and that further material functionalization is easily possible, including e.g., antibody-targeting of MB to BBB endothelial cells, and co-incorporating both contrast agents and drugs within the MB shell. Therefore, and also because it has become increasingly apparent that external means to open up the BBB are needed to enable more efficient and safe (macromolecular) drug delivery to the brain, we suggest that theranostic MB-based materials hold significant potential for individualizing and improving drug delivery to the brain.

3. Conclusion

This study shows that polymer-based MB, containing USPIO nanoparticles within their shell, can be employed to at the same time mediate and monitor BBB permeation. External means to temporally and spatially control BBB opening are considered to be important for individualizing and improving interventions in case of Alzheimer's disease, Parkinson's disease, and brain tumors, as these pathologies require systemic treatment with relatively large drug molecules (such as growth factors and antibodies; which because of an intact BBB do not efficiently reach the target site upon i.v. injection). Materials and methods enabling safe and efficient drug delivery across the BBB, ideally in an image-guided, targeted and triggered manner, consequently seem to hold significant potential for treating CNS disorders.

4. Experimental Section

Materials: *n*-butyl-cyanoacrylate (BCA) was obtained from Special Polymer Ltd, potassium ferrocyanide from AppliChem, and iron(III) chloride, iron(II)chloride tetrahydrate, FITC-dextran (70 kDa), Triton X-100 and Nuclear Fast Red solution from Sigma Aldrich. Ammonium hydroxide solution ($NH_3{\cdot}H_2O$, 25%) was obtained from Carl Roth GmbH, rhodamine-labeled RicinusCommunis Agglutinin I (rhodamine-lectin) from Vector Laboratories, Dulbecco's PBS from Life Technologies Corporation, 0.9 % saline and heparin-sodium from Braun, Tissue-Tek OCT Compound from Sakura Finetek Europe, and Resovist from Bayer Vital GmbH.

Synthesis and Characterization of USPIO and USPIO-MB: Ultrasmall super-paramagnetic iron oxide (USPIO) nanoparticles were prepared using a standard co-precipitation method of ferrous and ferric salts.[31] Briefly, $FeCl_3$ (16 mmol; 2.66 g) and $FeCl_2{\cdot}4H_2O$ (8 mmol; 1.63 g) were dissolved in deionized water. An aqueous ammonia solution (25%, $NH_3{\cdot}H_2O$, 4 mL) was then added drop-wise, followed by 10 min of vigorous stirring at 1500 rpm. After stirring, a permanent magnet was used to isolate the precipitated iron oxide nanoparticles, which were washed three times by re-dispersion in deionized water. The purified USPIO were physicochemically analyzed and subsequently stored in 40 mL of diluted HCl (0.02 M)[28]: The properties of the USPIO nanoparticles were: core size (as determined by transmission electron microscopy) = 5.5 ± 1.1 nm; hydrodynamic diameter and polydispersity (as determined by dynamic light scattering, in HEPES buffer, pH 7) = 252 ± 66 nm and 0.35, respectively; zeta potential (as determined using nanosizer, at pH 7) = 18.9 ± 2.5; molar ratio Fe^{2+}:Fe^{3+} = 1:2; and crystallinity (as determined using X-ray diffraction) = typical highly crystalline magnetite diffraction pattern, in line with JCPDS No. 19.0629. The longitudinal (r_1) and transversal (r_2) relaxivity of the nanoparticles could not be determined, because of aggregation in water at pH 7, which results in susceptibility artifacts.[32] MB with and without USPIO nanoparticles were synthesized as previously described.[33] USPIO-MB were synthesized by adding 3 mL of *n*-butyl-cyanoacrylate (BCA) monomer to an aqueous solution containing 1% (w/v) triton X-100 and 225 mg of pre-synthesized USPIO nanoparticles; regular MB were prepared similarly, but without USPIO nanoparticles in solution.[21] The mixture was stirred for 60 min at 10 000 using an Ultra-turrax mixer (IKA-Werke), giving rise to PBCA-MB containing USPIO in their shell. Subsequently, USPIO-MB were purified and size-isolated by two sequential rounds of centrifugation at 500 rpm for 10 min. After each centrifugation step, the MB were re-dispersed in an aqueous solution containing 0.02% (w/v) triton X-100. The mean diameter, size distribution and concentration of the USPIO-MB were analyzed using a Multisizer 3 (Beckman Coulter). The average shell thickness (determined on the basis of 50 individual MB), shape and surface morphology of the MB were visualized using cryo-scanning electron microscopy (FESEM, Hitachi-S4800). The encapsulation of USPIO into the MB shell was visualized using transmission electron microscopy (TEM; Philips EM400T). The iron concentration in USPIO-MB was analyzed using inductively coupled plasma mass spectrometry (ICP-MS; Elan-DRCII; Perkin Elmer). This was done

in triplicate, in a solution containing 10^8 MB. The reported value and the standard deviation (Supporting Information Table S1) therefore represent the intra-batch variability, rather than the variability in the amount of USPIO per individual MB. The colloidal stability of the MB in solution at 25 °C and pH 7 was evaluated by means of zeta potential measurement using a Malvern zetasizer (Nano ZS). In this context, the electrophoretic mobility was measured and the zeta potential calculated using the Henry's equation. Similarly, to evaluate colloidal stability, a direct measurement of the creaming velocity was performed at pH 7.4 and 25 °C using a separation analyzer LUMiFuge (LUM GmbH). The data was analyzed using SEPview software and the experimentally obtained creaming velocities extrapolated to 1xg to obtain the creaming velocities at ambient conditions.

Animal Model and In Vivo Experiments: All animal experiments were approved by a governmental review committee on animal care. Eight-weeks old CD-1 nude mice were obtained from Charles River Laboratories. Mice were anesthetized using isoflurane via a nose cone. Thirty-five animals were used, subdivided into 7 groups of 5 animals. Three groups received USPIO-MB plus US for 1, 5 or 30 min, three others received US alone, for 1, 5 or 30 min. One group received only USPIO-MB. All animals were initially examined with MRI (MRI-Pre; to obtain baseline R_2*-values), directly followed by the i.v. injection of 70 kDa FITC-dextran at a dose of 200 mg kg^{-1} in 0.9% saline. Then, in the US plus MB groups, 8.5×10^8 USPIO-MB were i.v. infused for 5 min into the tail vein. Total injection volumes never exceeded 150 µL. For the respective groups, mice were then exposed to transcranial Power Doppler US for 1, 5 or 30 min, and afterwards, always exactly 40 min after the injection of the USPIO-MB - a second MRI scan (MRI-Post) was performed. Two hours after the MRI-Post-scan, 250 I.U. heparin were injected i.p., followed by an i.v. injection of rhodamine-lectin into the tail vein at a dose of 15 mg kg^{-1}. Animals were sacrificed by inhalation of isoflurane in lethal dosage. Subsequent to exsanguination, a thoracotomy was performed to intracardially perfuse the mouse with 50 mL of phosphate-buffered saline at physiological conditions, to clear the vasculature of FITC-dextran. Fifteen additional mice received different combinations of regular PBCA-MB (i.e., without USPIO), US and free USPIO nanoparticles (i.e. Resovist; 50 µmol kg^{-1}). Three animals received standard MB with 5 min of US to assess the impact of MB destruction on hemorrhage. Four groups with 3 animals each were evaluated to analyze the effect of co-administration of Resovist alone, and with or without 5 min of US and/or regular MB.

Ultrasound: Ultrasound imaging and treatment was performed using the Vevo 2100US system (VisualSonics), connected to a MS250 transducer. Anaesthetized animals were mounted onto a heated custom-made mouse bed, supplying air and isoflurane through a nose cone. Power Doppler US was used at 16 MHz with a peak negative pressure of ≈3.6 MPa, resulting in a mechanical index of 0.9, to achieve a focal plane in the brain (≈3 mm below the skin). To apply US over the whole brain, the transducer was fixed, and the mouse bed was constantly moved through a gear, covering the whole skull in 3 s. The total US duration was set to 1, 5, or 30 min.

Magnetic Resonance Imaging: USPIO nanoparticle deposition after US-mediated USPIO-MB destruction, as well as morphological alterations and edema formation in the brain, were evaluated by MRI. MRI was performed using a Philips Achieva 3.0 T clinical MRI scanner, equipped with a mouse volume coil. For morphological imaging, a T_2-weighted turbo spin echo (TSE) sequence (TR = 2152 ms, TE = 100 ms, slice thickness = 1 mm, flip angle = 90 °, FOV = 22 mm × 22 mm × 20 mm, matrix size = 160 × 160), and a T_2* turbo field echo (TFE) with dual echo sequence (TR = 14 ms, TE_{first} = 4.6 ms, TE_{second} = 9.21 ms, slice thickness = 2 mm, flip angle = 15 °, FOV = 28 mm × 28 mm × 20 mm, matrix size = 116 x 117) were applied. For evaluation of edema formation, we used a fluid attenuated inversion recovery (FLAIR) sequence (TR = 11 000 ms, TE = 139.14 ms, slice thickness = 3 mm, flip angle = 90°, FOV = 20 mm × 38 mm × 21 mm, matrix size = 92 × 60). T_2*-relaxation times (T_2*) were determined using a T_2*-weighted multi-slice multi-shot fast-field gradient-echo sequence (TR = 1295 ms, TE range = 10–117.8 ms, delta TE = 7.7 ms, slice thickness = 1 mm, flip angle = 30°, FOV = 33 mm × 29 mm × 16 mm, matrix size 84 × 72). Images were acquired at 15 echo times, and T_2* was calculated by fitting an exponential curve of the signal amplitudes as a function of echo time for each pixel. For calculation of average brain R_2* (i.e., $1/T_2$*), regions of interest (ROI, based on >5000 voxels) were selected in coronary slices caudal of the olfactory bulb and frontal of the cerebellum. Subsequently, color-coded R_2*-maps were generated and overlaid on T_2*-weighted morphological images. Phantoms were prepared by mixing USPIO-containing or regular MB into a warm aqueous solution containing 2.5% gelatin (c = 50 MB μL^{-1}). Subsequently, 1 mL of the solution was filled into an Eppendorf tube and rapidly cooled down (–20 °C for 15 min). In another Eppendorf tube, prior to cooling, the MB were destroyed by sonication. The phantoms were measured in a knee coil (SENSE Flex M Philips, Netherlands). For morphological imaging, a T_2-weighted Turbo Spin Echo (TSE) sequence (TR = 846 ms, TE = 100 ms, slice thickness = 1 mm, flip angle = 90 °, FOV = 56 mm × 11 mm × 4 mm, matrix size = 160 × 160) was applied. T_2*-relaxation times (T_2*) were determined using a T_2*-weighted multi-slice multi-shot fast-field gradient-echo sequence (TR = 290 ms, TE range = 6–131 ms, delta TE = 4.2 ms, slice thickness = 1 mm, flip angle = 30°, FOV = 55 mm × 11 mm × 6 mm, matrix size = 176 × 176). Images were acquired at 30 echo times, and T_2* was calculated as described beforehand. Per phantom, 4 slices and 5 measurements per slice were performed. Quantification was performed using the Relaxation Maps Tool (Philips Research Laboratories).

Histological Evaluation: Brain tissue was harvested and mounted in Tissue-Tek O.C.T. compound. It was snap-frozen at –80 °C and cut into transversal sections of 8 µm thickness, using a CM3050S cryostat (Leica Microsystems). For each animal, 3 slices were examined, each 100 µm apart. For rhodamine-lectin-stained vessels and FITC-dextran extravasation, ten images per slice were recorded by 2D fluorescence microscopy (FM) at 400-fold magnification with an AxioImager M2 microscope, equipped with an AxioCam MR3- and an AxioCam ICc-1-camera (Carl Zeiss). Images were randomly chosen from the cortical region of the brain. Automated quantification was performed for thirty images per brain. Based on the mean signal intensity of FITC-dextran in the concentric rings of these thirty images, each brain resulted in a graph depicting average signal intensity around a vessel as a function of distance to the vessel (in 1.6 µm steps, equivalent to 10 pixels). For 3D visualization, transversal sections of 70 µm thickness were imaged using a pulsed Ti-sapphire laser MaiTaiDeepSee (Spectra Physics), attached to the upright two-photon laser scanning microscope (2PM) system Fluoview 1000MPE (Olympus), with a 20X water dipping objective (1.05 NA, WD2.0). For excitation, the laser was tuned to a wavelength of 800 nm at 5% output. Emitted fluorescent signals were detected with two sensitive non-de-scanned photomultiplier tubes. The emission of FITC-dextran and rhodamine-lectin was collected at 495–540 nm and 575–630 nm, respectively. Series of subsequent xy-frames with 1024 × 1024 pixels in fifty 1 µm z-steps were obtained for structural 3D reconstruction of the vasculature. Image analysis was conducted using the imaging software Imaris 7.4 (Bitplane). Definiens Developer XD 2.0.4 was used for automated histological evaluation. To confirm USPIO deposition in the brain, Prussian Blue stainings were performed. To this end, after methanol fixation at –20 °C, brain sections were incubated for 5 min with a 10 % aqueous solution of $K_4Fe(CN)_6$, and then with a 1:1 mixture of 10% $K_4Fe(CN)_6$ and 20% HCl for 30 min. Tissues were counterstained with Nuclear Fast Red for 10 min. Subsequently, the sections were washed with water and mounted with coverslips.

Statistical Analysis: All results are represented as averages ± standard error of the mean. For intra-individual changes in R_2*, statistical significance was examined by using the paired two-tailed Student's t-test. Based on the large amount of histological and MRI data obtained, evaluation of the statistical difference between the individual groups was performed using analysis of variance (ANOVA). The least significant difference (LSD) test for post-hoc evaluation was employed. All calculations were performed using IBM SPSS Statistics 20. $p < 0.05$ was considered to represent statistical significance.

Acknowledgements

T.L. and P.K. contributed equally to this work. The authors acknowledge M. Weiler, S. Arns, A. Rix, D. Moeckel, Dr. Z. Liu and the core facility "Two-Photon Imaging" at the Interdisciplinary Center for Clinical Research (IZKF) at RWTH Aachen University Clinic for technical assistance. The European Research Council (Starting Grant 309495-NeoNano), the European Union 7th Framework Programme (COST-Action TD1004 and Grant agreement no. NMP4-LA-2013-310451), the DFG (LA 2937/1-2), the ERS Boost Fund at RWTH Aachen, the German Federal State of North Rhine Westfalia (HighTech.NRW/EU-Ziel2-Programm (EFRE;2007-2013): "ForSaTum") and the Helmholtz-Society (Portfolio Grant "Technologie und Medizin: Multimodale Bildgebung zur Aufklärung des In-vivo-Verhaltens von Polymeren Biomaterialien") are gratefully acknowledged for financial support.

Received: April 14, 2014
Revised: July 23, 2014
Published online: September 16, 2014

[1] G. Miller, *Science* **2002**, *297*, 1116.
[2] W. M. Pardridge, *Drug Discovery Today* **2007**, *12*, 54.
[3] N. J. Abbott, L. Rönnbäck, E. Hansson, *Nat. Rev. Neurosci.* **2006**, *7*, 41.
[4] A. Armulik, G. Genové, M. Mäe, M. H. Nisancioglu, E. Wallgard, C. Niaudet, L. He, J. Norlin, P. Lindblom, K. Strittmatter, B. R. Johansson, C. Betsholtz, *Nature* **2010**, *468*, 557.
[5] R. C. Brown, R. D. Egleton, T. P. Davis, *Brain Res.* **2004**, *1014*, 221.
[6] C. W. Gan, S. S. Feng, *Biomaterials* **2010**, *31*, 7748.
[7] S. Wohlfart, S. Gelperina, J. Kreuter, *J. Controlled Release* **2012**, *161*, 264.
[8] S. Krol, R. Macrez, F. Docagne, G. Defer, S. Laurent, M. Rahman, M. J. Hajipour, P. G. Kehoe, M. Mahmoudi, *Chem. Rev.* **2013**, *113*, 1877.
[9] K. Hynynen, N. McDannold, N. A. Sheikov, F. A. Jolesz, N. Vykhodtseva, *Neuroimage* **2005**, *24*, 12.
[10] M. Kinoshita, N. McDannold, F. A. Jolesz, K. Hynynen, *Proc. Natl. Acad. Sci. USA* **2006**, *103*, 11719.
[11] E. J. Park, Y. Z. Zhang, N. Vykhodtseva, N. McDannold, *J. Controlled Release* **2012**, *163*, 277.
[12] A. Burgess, K. Hynynen, *ACS Chem. Neurosci.* **2013**, *4*, 519.
[13] Y. Z. Zhao, C. T. Lu, X. K. Li, J. Cai, *J Expert. Opin. Drug Delivery* **2013**, *10*, 987.
[14] E. G. Schutt, D. H. Klein, R. M. Mattrey, J. G. Riess, *Angew. Chem. Int. Ed.* **2003**, *42*, 3218.
[15] K. Ferrara, R. Pollard, M. Borden, *Annu. Rev. Biomed. Eng.* **2007**, *9*, 415.
[16] S. Hernot, A. L. Klibanov, *Adv. Drug. Delivery Rev.* **2008**, *60*, 1153.
[17] E. Huynh, J. F. Lovell, B. L. Helfield, M. Jeon, C. Kim, D. E. Goertz, B. C. Wilson, G. Zheng, *J. Am. Chem. Soc.* **2012**, *134*, 16464.
[18] S. Fokong, B. Theek, Z. Wu, P. Koczera, L. Appold, S. Jorge, U. Resch-Genger, M. van Zandvoort, G. Storm, F. Kiessling, T. Lammers, *J. Controlled Release* **2012**, *163*, 75.
[19] F. Kiessling, S. Fokong, P. Koczera, W. Lederle, T. Lammers, *J. Nucl. Med.* **2012**, *53*, 345.
[20] C. H. Fan, C. Y. Ting, H. J. Lin, C. H. Wang, H. L. Liu, T. C. Yen, C. K. Yeh, *Biomaterials* **2013**, *34*, 3706.
[21] Z. Liu, T. Lammers, J. Ehling, S. Fokong, J. Bornemann, F. Kiessling, J. Gätjens, *Biomaterials* **2011**, *32*, 6155.
[22] M. Palmowski, B. Morgenstern, P. Hauff, M. Reinhardt, J. Huppert, M. Maurer, E. C. Woenne, S. Doerk, G. Ladewig, J. W. Jenne, S. Delorme, L. Grenacher, P. Hallscheidt, G. W. Kauffmann, W. Semmler, F. Kiessling, *Invest. Radiol.* **2008**, *43*, 162.
[23] T. Lammers, S. Aime, W. E. Hennink, G. Storm, F. Kiessling. *Acc. Chem. Res.* **2011**, *44*, 1029.
[24] A. Tiwari, *Advanced Healthcare Materials*, WILEY-Scrivener Publishing LLC, Hoboken, NJ **2013**.
[25] A. Tiwari, *Bioengineered Nanomaterials*, CRC Press, Boca Raton, FL, **2013**.
[26] A. Tiwari, *Nanomaterials in Drug Delivery, Imaging and Tissue Engineering*, WILEY-Scrivener Publishing LLC, Hoboken, NJ, **2014**.
[27] C. Vauthier, C. Dubernet, E. Fattal, H. Pinto-Alphandary, P. Couvreur, *Adv. Drug Delivery Rev.* **2003**, *55*, 519.
[28] S. Laurent, D. Forge, M. Port, A. Roch, C. Robic, L. Vander Elst, R. N. Muller, *Chem. Rev.* **2008**, *108*, 2064.
[29] J. J. Choi, K. Selert, F. Vlachos, A. Wong, E. E. Konofagou, *Proc. Natl. Acad. Sci. USA* **2011**, *108*, 16539.
[30] B. Marty, B. Larrat, M. Van Landeghem, C. Robic, P. Robert, M. Port, D. Le Bihan, M. Pernot, M. Tanter, F. Lethimonnier, S. Mériaux, *J. Cereb. Blood Flow Metab.* **2012**, *32*, 1948.
[31] S. E. Khalafalla, G. W. Reimers, *IEEE Trans. Magn.* **1980**, *16*, 178.
[32] J. Jayapaul, M. Hodenius, S. Arns, W. Lederle, T. Lammers, P. Comba, F. Kiessling, J. Gätjens, *Biomaterials* **2011**, *32*, 5863.
[33] S. Fokong, M. Siepmann, Z. Liu, G. Schmitz, F. Kiessling, J. Gaetjens, *Ultrasound Med. Biol.* **2011**, *37*, 1622.